Geometry Effects on Flow Transition in Multilouvered Fins – Onset, Propagation, and Characteristic Frequencies

D. K. Tafti and X. Zhang

ACRC TR-174 August 2000

For additional information:

Air Conditioning and Refrigeration Center
University of Illinois
Mechanical & Industrial Engineering Dept.
1206 West Green Street
Urbana, IL 61801

(217) 333-3115

Prepared as part of ACRC Project 94
Computational Study Of Multilouvered Fin Heat Exchangers
D. K. Tafti, Principal Investigator

The Air Conditioning and Refrigeration Center was founded in 1988 with a grant from the estate of Richard W. Kritzer, the founder of Peerless of America Inc. A State of Illinois Technology Challenge Grant helped build the laboratory facilities. The ACRC receives continuing support from the Richard W. Kritzer Endowment and the National Science Foundation. The following organizations have also become sponsors of the Center.

Amana Refrigeration, Inc.
Arçelik A. S.
Brazeway, Inc.
Carrier Corporation
Copeland Corporation
DaimlerChrysler Corporation
Delphi Harrison Thermal Systems
Frigidaire Company
General Electric Company
General Motors Corporation
Hill PHOENIX
Honeywell, Inc.
Hussmann Corporation
Hydro Aluminum Adrian, Inc.
Indiana Tube Corporation
Invensys Climate Controls
Lennox International, Inc.
Modine Manufacturing Co.
Parker Hannifin Corporation
Peerless of America, Inc.
The Trane Company
Thermo King Corporation
Valeo, Inc.
Visteon Automotive Systems
Whirlpool Corporation
Wolverine Tube, Inc.
York International, Inc.

For additional information:

Air Conditioning & Refrigeration Center
Mechanical & Industrial Engineering Dept.
University of Illinois
1206 West Green Street
Urbana, IL 61801

217 333 3115

GEOMETRY EFFECTS ON FLOW TRANSITION IN MULTILOUVERED FINS – ONSET, PROPAGATION, AND CHARACTERISTIC FREQUENCIES

D. K. Tafti
X. Zhang

National Center for Supercomputing Applications
University of Illinois at Urbana-Champaign
Urbana, IL 61801
USA

Running Head: *Geometry effects on transition in multilouvered fins*

ABSTRACT

The effect of fin pitch, louver angle and thickness, and flow depth on the onset, propagation, and characteristic frequencies of instabilities in multilouvered fins is investigated. The initial instability appears in the wake of the exit louver. Subsequently, instabilities are established in the interior of the louver bank which spread upstream as the Reynolds number increases. It is shown that the interior instabilities are completely independent of the exit wake instability. On the other hand, the exit wake instability is not only dependent on the exit louver geometry but also on the internal geometry of the louver bank. Increasing louver thickness and angle increases the propensity of the flow to become unstable. Increasing fin pitch, louver angle, and thickness enhances the propagation of instabilities into the array. It is shown that the characteristic frequencies in the interior of the louver bank, scale with the fin pitch rather than the louver thickness or louver pitch. The exit wake frequencies, on the other hand scale with the projected length of the exit louver in the flow direction. A simplified model for estimating the onset of instabilities in the interior of the louver bank is proposed.

NOMENCLATURE

b	non-dimensional fin thickness $\left(b^* / L_p^*\right)$
f	non-dimensional characteristic frequency
F_p	non-dimensional fin pitch (F_p^* / L_p^*)
F_d	non-dimensional flow depth (F_d^* / L_p^*)
L_p^*	dimensional louver pitch (characteristic length scale)
Re_{in}	Reynolds number $(u_{in}^* L_p^* / \nu)$
Re_s	Reynolds number $\left(u_s^* s^* / \nu\right)$
S_1,S_2	non-dimensional entrance/exit and redirection louver dimensions
s^*	dimensional distance along flow path traversed
T	temperature
u_{in}^*	dimensional inlet velocity (characteristic velocity scale)
u_s^*	dimensional velocity component in flow direction

Greek symbols

α	flow angle
θ	louver angle
ν	kinematic viscosity

Superscripts

*	dimensional quantities

Subscripts

c	critical Reynolds number
f	based on fin
i	pertaining to interior of louver bank
in	based on inlet
w	pertaining to exit wake
i	pertaining to interior of louver bank

INTRODUCTION

Air-side heat transfer augmentation through the use of multilouvered fin finds wide spread use in compact heat exchangers in the automobile and HVAC industry. Three factors influence the heat transfer coefficient and heat capacity of multilouvered fins. First among them is the predominant flow direction in the louver bank. When the bulk of the flow in the louver bank is aligned with the streamwise direction, it is referred to as duct directed flow. This was first recognized by Davenport [1] and studied by other researchers in the field [2]. Duct directed flow has a detrimental effect on the heat capacity and heat transfer coefficient, since a small fraction of the fluid flows between louver passages. On the other hand, louver directed flow has a large positive impact on the heat transfer coefficient. High Reynolds numbers, large louver angles, small fin pitches, and large louver pitches are conducive to louver directed flow. Because of the compactness of multilouvered banks, thermal wake interference also has a significant impact on the heat capacity [3]. Zhang and Tafti [4] classified two types of thermal wake effects. Intra-fin interference occurs between louvers in the same fin, and is dominant when the flow is duct directed. Inter-fin interference occurs between adjacent rows of fins when the flow is louver directed. Both intra- and inter- types can have a large effect on the total heat capacity of the fin, whereas the latter does not have a large effect on the heat transfer coefficient. Finally, the development of self sustained flow oscillations, which lead to large scale vortical structures in the louver bank, has the effect of augmenting the heat transfer coefficient [5,6].

Our objective in this paper is to study the comprehensive effect of multilouver geometrical parameters on the onset and propagation of instabilities, and on the characteristic frequencies observed in the louver bank. In addition to heat transfer augmentation, the unsteady aspects of the flowfield have important applications in understanding noise generation in heat exchanger cores. There are a few isolated studies in the literature which have studied the onset of flow instabilities in heat exchanger cores. Mochizuki and Yagi [7] experimentally investigated the effect of different flow depths in model offset strip fin like cores. They investigated the onset of instabilities on single confined plates in a channel up to 18 columns with multiple rows of fins in a staggered arrangement, which is more representative of a real heat exchanger core. They found that instabilities always appeared in the wake of the array which then moved upstream into the array. They found multiple characteristic frequencies present in arrays with less than 8 columns, while found a single characteristic frequency as the number of columns increased beyond 8, thus indicating that flow oscillations in a large array are influenced by factors other than individual flat plates. The single characteristic Strouhal number of 0.13 was independent of the Reynolds number and the number of columns. Dejong and Jacobi [8] have also speculated from their flow visualization studies that instabilities first appeared at the trailing edge of the last row of plates, which then propagated upstream. The same authors observed a similar pattern in multilouvered arrays [9]. Springer and Thole [10,11] have measured the characteristic frequencies in three louver geometries with different fin pitch to louver pitch ratios. Tafti et al. [12], used high fidelity numerical simulations in a single louver geometry to map the onset of instabilities, spatial propagation and characteristic frequencies. In agreement with experimental studies they found that the initial instability appeared in the wake of the exit louver, which then spread upstream into the interior of the louver bank. They also found that the unsteadiness in the louver bank was characterized by a single characteristic frequency. Curiously, once established, the characteristic frequency was also present in regions of the bank where no large-scale unsteadiness was observed.

In this paper we extend our earlier study to multiple louver geometries. We study the effect of fin pitch, louver angle, louver thickness, and flow depth on the initial instability, its propagation and characteristic frequencies. We also propose a model to estimate the onset of instabilities in a louver bank and introduce relevant length and velocity scales for scaling characteristic frequencies. Finally, we perform numerical experiments to estimate the extent to which the exit wake instability affects the instabilities in the louver bank, and conversely the effect of the interior louver geometry on the exit wake instability.

GOVERNING EQUATIONS AND MATHEMATICAL FORMULATION

To calculate the flow and thermal fields in the array, we map the Navier-Stokes and energy equations from physical to logical/computational space by a boundary conforming transformation. The governing equations for momentum and energy conservation are discretized with a conservative finite-volume formulation on a non-staggered mesh. Both, convection and viscous terms are approximated by second-order central-difference schemes. The computational domain, shown in Fig. 1(a), consists of one entire row of the louvered fin geometry allowing for the inclusion of entrance and exit effects in the flow direction. Periodic boundary conditions are applied in the transverse direction whereas Dirichlet boundary conditions are specified at the entrance to the array. To facilitate the calculation of the whole fin, we use a structured multi-block formulation in the streamwise direction.

The governing equations are non-dimensionalized by a characteristic length given by the louver pitch L_p^*, a characteristic velocity scale given by the inlet velocity to the array (u_{in}) and a temperature scale given by ($T_f^* - T_{in}^*$), where T_f^* is the specified fin surface temperature. The non-dimensionalization results in a characteristic Reynolds number $\mathrm{Re} = \mathrm{Re}_{in} = u_{in}^* L_p^* / \nu$, with boundary conditions $u_{in} = 1, T_{in} = 0$ at the entrance to the computational domain. The Prandtl number is fixed at 0.7 for air. At the fin surface, no slip, no penetration boundary conditions for the velocity field, and $T_f = 1$ for the temperature field are applied. Due to the recovering nature of the flow at the array exit, a convective boundary conditions is used at outflow boundary nodes. More details about the governing equations, time-integration algorithm, numerical discretization, treatment of boundary and louver surface conditions, and validation of the computer program can be found in Tafti et al. [13,14].

COMPUTATIONAL DETAILS

The basic configuration used in all calculations consists of an entrance and exit louver with four louvers on either side of the center or redirection louver. For the entrance and exit louvers, S_1 = 1, and for the redirection louver, S_2 = 1 were fixed in all the calculations. Table 1 summarizes the different louver geometries studied. Cases 1 to 4 have a fin pitch ratio (F_p) of 1.0, whereas cases 5 to 8 have a fin pitch ratio of 1.5. Four louver angles (θ) ranging from 15 to 30 degrees in increments of 5 degrees are investigated for each fin pitch. The nominal louver thickness ratio (b) and flow depth (F_d) are 0.1 and 13, respectively. Effect of louver thickness ratios of 0.05 and 0.15 are studied in cases 1(a-b) and 3(a-b) for F_p = 1.0 and θ = 30 and 20 degrees, respectively. The effect of increasing flow depth is studied in case 5(a), in which the number of louvers are increased from 8 to 12.

Fig. 1(b) shows the computational domain which is resolved by 15 computational blocks, one for each louver, two each for the entrance, exit and redirection louver, and an exit domain which extends approximately 5.5 non-dimensional units downstream (or about 55 louver thickness units) of the exit louver. Each block is resolved by 96x96 finite-volume cells. In Tafti et al. [12] we compared results on grids of 64x64 and 96x96 per computational block to find that there were some minor differences in the characteristic frequencies (<5%) and the onset and spread of instabilities between the two grids. To further establish grid independency for the results reported in this paper, which use 96x96 cells per block, we conducted an additional, completely independent calculation on a 128x128 grid per computational block for F_p = 1.5 and Re_{in} =1000. Fig. 2 (a-b) compare the time averaged flow field on the entrance louver and louver number 5, which is downstream of the redirection louver. The 96x96 grid calculation reproduces the recirculation regions with accuracy and the results are identical to the fine grid calculation. In addition, there is excellent agreement in characteristic frequencies calculated by the two resolutions. These are shown in Fig. 2 (c-d) at two locations in the multilouvered array. The time averaged heat transfer coefficient on the 96x96 grid is within 1% of the fine grid calculation.

ONSET OF INSTABILITIES

In our earlier study [12] for F_p =1.0 and θ = 30 degrees, it was found that the initial instability appeared in the wake of the exit louver at Re_{in} = 400. Subsequently, additional instabilities were established in the interior of the array near the exit. There was evidence of infiltration of the characteristic exit wake frequency into the interior before any instabilities appeared in the interior. The interior instabilities manifested themselves as leading edge shear layer or Kelvin-Helmholtz type instabilities and louver wake instabilities. With an increase in Reynolds number the instabilities then propagated upstream. A similar sequence of events was found to occur in all the cases studied in this paper.

Fig. 3(a-b) show the formation of the exit wake instability for a louver angle of 30 degrees and F_p = 1.0 and 1.5 at Re_{in} = 400. In both cases, the shear layer from the top leading edge interacts with that formed at the bottom trailing edge and becomes unstable in the wake[1]. Fig. 3 shows the corresponding time signals and frequency spectra for the two cases with characteristic peaks exhibited at 0.87 and 0.7, respectively.

Figure 4(a) plots $\mathrm{Re}_{c,w}$, the critical Reynolds number at which the exit wake becomes unstable to the nearest hundred. The fin pitch ratio does not have a large effect on $\mathrm{Re}_{c,w}$ except at a louver angle of 15 degrees, at which the smaller fin pitch exhibits an earlier onset of flow oscillations in the wake. On the other hand, louver angle has a large effect on the onset of the wake instability – it occurs as early as $\mathrm{Re}_{c,w}$ = 400 at θ = 30 degrees but is delayed to $\mathrm{Re}_{c,w}$ = 1200 for θ = 15 degrees.

[1] We define the initial appearance of this instability when the characteristic Von Karman vortex street is visible within the calculation domain. In a larger calculation domain, the instability would develop further downstream earlier than reported in this study.

Figure 4(b) plots the onset of the wake instability as a function of louver thickness for F_p =1.0 and θ= 30 and 20 degrees. An increase in thickness decreases $\mathrm{Re}_{c,w}$ for both louver angles. However, the effect is much stronger for the smaller louver angle as evidenced by the larger slope for θ= 20 degrees. For b = 0.05, the wake remains stable up to a Re_{in} = 1200, which was the maximum Reynolds number calculated. It is conjectured that as the fin pitch increases, fin thickness will have a smaller effect on the onset of transition.

On the appearance of the exit wake instability, the characteristic frequency from the exit wake is found to penetrate the interior of the multilouvered array. Fig. 5(a-b) show examples of this for F_p =1.5 and θ= 30 degrees. On the appearance of the exit wake instability at Re_{in} = 400, flow oscillations of the same characteristic frequency, albeit of smaller amplitudes, are found to penetrate the interior of the array as shown in Fig. 5(a-b) for Re_{in} = 500 and 600, respectively. At Re_{in} = 700, however, there is a distinct shift in the characteristic frequency, which now changes to 1.25. At this point, interior instabilities either as louver wake instabilities or louver leading edge shear layer instabilities, which are quite distinct from the exit wake instability, start establishing themselves[2]. This is shown in Fig. 5(c). Interestingly, even though the instability has established itself only on louvers near the exit, its effect can be felt throughout the louver bank as evidenced by the penetration of the characteristic frequency all the way upstream to louver 1.

The critical Reynolds number for the interior instability is plotted in Fig. 6(a) for the two fin pitches and louver angles. Similar to the trends in Fig. 4(a), it is found that the fin pitch does not have a large effect on the onset, whereas a large louver angle exhibits much lower $\mathrm{Re}_{c,i}$. For θ= 15 degrees, the interior instability does not appear till Re_{in} =1200, the largest Reynolds number calculated. An increase in fin thickness lowers $\mathrm{Re}_{c,i}$ as shown in Fig. 6(b) for θ=30 and 20 degrees. However, unlike its effect on the wake instability, both louver angles exhibit similar slopes. For θ= 20 degrees and b = 0.05, the flow was stable up to Re_{in} = 1200. Fig. 6(c) plots the effect of increasing flow depth on the wake and interior instability. It is found that increasing flow depth hastens the development of both instabilities. The wake instability appears at Re_{in} = 300 versus Re_{in} = 400 for the smaller flow depth and the interior instability appears earlier at $\mathrm{Re}_{c,i}$ = 600 compared to Re_{in} = 700 for the smaller flow depth.

An early transition with increasing flow depth indicates that the onset of instabilities is dependent on the distance a fluid element travels in the array. To quantify this effect, we define a Reynolds number based on the flow distance traversed by a fluid element and a velocity parallel to this direction. By doing this we shift our focus from individual louvers to a collection of louvers, which form a flow conduit or duct as illustrated in Fig. 7(a). Each louver is akin to a large roughness element, which perturbs the flow. The degree of perturbation is a complex function of louver geometry. As a fluid element traverses through the duct, the cumulative effect of these perturbations causes the flow to develop instabilities at some downstream location in the duct. The instability manifests itself around a single louver in the form of a leading edge shear layer instability or as a louver wake instability. This view of the transition mechanism is very consistent with the fact that in arrays of fins, the initial instability is always found to start at the downstream end of the array, which then propagates upstream as the Reynolds number increases. This has been seen in experiments of staggered plate arrays [7,8], and multilouvered arrays [9] and also in our computations.

To construct a simple predictive model to estimate the onset of instabilities we assume that the flow angle is a constant and the fluid element traverses the sides of a triangle as shown in Fig. 7(a). We define a Reynolds number based on s^*, the flow distance traversed as:

$$\mathrm{Re}_s = \mathrm{Re}_{in} \times \frac{u_s^*}{u_{in}^*} \times \frac{s^*}{L_p^*}, \qquad (1)$$

where

$$\frac{s^*}{L_p^*} = \frac{2n}{\cos\beta} \qquad (2)$$

[2] The Reynolds number at which we observe the characteristic shift in frequency is taken to be the critical Reynolds number for the internal instabilities.

and by conservation of mass

$$\frac{u_s^*}{u_{in}^*} = \frac{F_p^*}{F_p^* \cos\beta - b^*} \tag{3}$$

Here n is an integer value corresponding to the number of louver lengths from the end of the entrance louver to the mid-point of the re-direction louver. For the two flow depths studied, n = 5 and 7, respectively. The flow angle β could be taken as the actual average flow angle calculated from the flow efficiency or the louver angle (θ). Since we want to use the above expression as an estimation tool for the onset of unsteadiness in the array, we prefer to use the louver angle. Applying the above expression to $\mathrm{Re}_{c,i}$ = 700 and 600 for the two cases with varying flow depths, we obtain values of $\mathrm{Re}_s = 10{,}000$ and 12,000, respectively. However, we note that low amplitude oscillations are present in the interior at Re_{in} = 500 for the larger flow depth, which subsequently would give $\mathrm{Re}_s = 10{,}000$, the same as the smaller flow depth. Hence, knowing the onset of internal array instabilities for a given geometry and flow depth, we can make use of the above equations to estimate the onset in terms of Re_{in} when the flow depth is either increased or decreased.

We extend this model to other geometries by which we obtain a critical Reynolds number based on the flow path traversed for the onset of internal array instabilities. Fig. 7(b) plots the calculated Re_s versus louver angle for the different geometries tested. We find that the critical Reynolds number increases as the louver angle decreases. This should be expected because as the louver angle tends to zero, the flow geometry approaches a smooth developing channel flow. For louver angles between 20 and 30 degrees and thickness ratios greater than or equal to 0.1, the onset of interior instabilities occurs between Re_s = 10,000 and 12000. For louver angles less than 20 degrees, transition is delayed till Re_s = 14000. Lowering the louver thickness to 0.05 delays transition beyond Re_s > 17000.

Also shown in Fig. 7(b) is the onset of transition as measured by Dejong and Jacobi [9] in different multilouvered geometries. Their geometries are characterized by a larger flow depth (n = 8, L_p^* = 11.9 mm) than in our study. The three geometries which they studied had a thickness ratio of 0.1 with F_p = 1.09, θ=18; F_p = 1.2, θ= 22; and F_p = 1.09, θ= 28, respectively. The critical Reynolds numbers (based on louver pitch and flow velocity at minimum cross-sectional area) which they cite (their Fig. 4.6) are quite different when compared to $Re_{c,i}$ for similar louver geometries in our calculations. However, when cast in terms of Re_s, there is very good agreement in the general trends although their values are somewhat higher than the ones observed in this study. Since their observations were based on dye injection and flow visualization, it is possible that they sensed transition later than the numerical calculations.

We extended the same estimation criterion to the onset of instabilities in an array of staggered plates. Dejong and Jacobi [8] found the onset of instabilities in their 8 stage array at a Reynolds number (based on plate thickness and flow velocity at minimum cross-sectional area) of 100, whereas Mochizuki and Yagi [7] in a 18 stage array found the onset of instabilities at the exit of the array at a similarly defined Reynolds number of 50. For reference, F_p = 0.5, b = 0.125, in [8] whereas in [7], F_p = 1.33 and b = 0.133 (non-dimensionalized by chord of plate). However, when converted to Re_s, both Dejong and Jacobi [8] and Mochizuki and Yagi [7] exhibit similar values of 6550 and 6750, respectively. This result indicates that a staggered plate array is more prone to instabilities than a louvered array and a shorter flow depth is required by the former for the onset of instabilities.

The use of Re_s to calculate the onset of instabilities in fin arrays is a simplification of the complex flow dynamics. However, as illustrated, it can provide a reasonably good tool in estimating the onset of instabilities.

PROPAGATION OF INSTABILITIES INTO LOUVER BANK

Once the interior instability is established near the exit of the multilouvered array it propagates upstream into the louver bank. The rate of propagation is dependent on the louver geometry. For example, Fig. 8 plots the instantaneous vorticity contours for F_p = 1.0 and 1.5 and θ=30 degrees. At Re_{in} = 400, the exit wake Von Karman vortex street is visible for both geometries. However, at Re_{in} =800, the flowfield in the interior of the array exhibits large differences between the two fin pitches. For the larger fin pitch, the instability has progressed all the way to the upstream end of the louver bank as evidenced by the wavy wakes behind louvers near the entrance. On the other hand, for the smaller fin pitch, the flow is quite stable except for some wake waviness on louvers near the exit. The

faster propagation of instabilities for the larger fin pitch can also be surmised from the measurements of Springer and Thole [11], in which they found an earlier onset of unsteadiness with an increase in fin pitch.

The rate of propagation of instabilities for different louver angles is summarized in Fig. 9(a). The horizontal axis depicts the louver number to which the instability has propagated for a given Reynolds number. The exit louver depicts the initial exit wake instability. A horizontal line indicates infinitely fast propagation while a vertical line depicts an infinitely slow propagation. For $\theta = 30$ degrees, the instabilities propagate upstream much faster for $F_p = 1.5$ than for $F_p = 1.0$. As the louver angle decreases to 25 degrees, the initial rate of propagation in the downstream half of the array is faster for $F_p = 1.5$, but is comparable to $F_p = 1.0$ in the upstream half of the array. As the louver angle decreases to 20 degrees, the rate of propagation is similar for both fin pitches. An increase in fin thickness not only initiates the interior instability earlier but also increases the rate of propagation upstream into the array. This is shown in Fig. 9(b). For $\theta = 30$ degrees, instabilities are established much more rapidly in the downstream half of the array for the thicker fins whereas the rate of spread is slower for the thinner fins. The same observation is made for the 20 degree louvers. Fig. 9(c) shows the effect of flow depth on the spread of instabilities. Interestingly, although the initial appearance of instabilities occurs earlier with an increase in flow depth, the spread of instabilities upstream is very similar in both cases. For example, at $Re_{in} = 700$, the instability in both cases has moved up to louver 7-8 and to louver 1 by $Re_{in} = 800$. This observation lends credence to our assertion in the previous section that the transition mechanism is a strong function of Re_s.

CHARACTERISTIC FREQUENCIES

Fig. 10(a-b) plot the effect of fin pitch and louver angle on characteristic frequencies in the wake of the exit louver and the interior of the array. The frequencies are non-dimensionalized by the inlet velocity and the louver pitch $\left(f = f^* L_p^* / u_{in}^*\right)$. For the wake the non-dimensional frequencies range from 0.7 to 1.2 and the interior frequencies range from 1.2 to 2.1. Also plotted in Fig. 10(b), are measured frequencies from Springer and Thole [11] for $b = 0.08$, $\theta = 27$ degrees, and $F_p = 0.76$, 0.91, and 1.52, respectively.

Curiously, for $F_p = 1.5$ and $\theta = 30$ degrees, we find that up to a Reynolds number of 900, the flow exhibits a characteristic frequency of 1.35 with superharmonics at 2.7, 4.05 and so on. Between $Re_{in} = 1000$ and 1200, the flow develops an additional subharmonic (period doubling), which establishes itself firmly at $Re_{in} = 1300$. Fig. 11(a) shows the frequency spectra at different locations in the array for $Re_{in} = 1000$. In the upstream half of the array (for example see louver 2), the temperature signal flip-flops between two states, one at a frequency of 1.4 and the other at half this value. Between $Re_{in} = 1100$ and 1200, the subharmonic component establishes itself in the downstream half of the array and finally reaches a stable state throughout the louver bank at $Re_{in} = 1300$, which is shown in Fig. 11(b). Hence in Fig. 10(b) we represent both frequencies for $Re_{in} > 900$ for this geometry. We also note that at $Re_{in} = 1000$, the flow is approaching a chaotic state in the downstream half of the array. Once the subharmonic component establishes itself at $Re_{in} = 1300$, the time signals once again exhibit an ordered state with characteristic peaks in the frequency spectra.

For both the wake and the interior we find that louver angle has a weak effect on the characteristic frequencies. The effect of increasing louver angle is somewhat discernable for the smaller fin pitch of $F_p = 1.0$ where it reduces the characteristic frequency. There is no discernable effect for the larger fin pitch. On the other hand, fin pitch has a much more substantial effect on the characteristic frequencies in the interior of the array and a smaller effect on the wake frequency – an increase in fin pitch decreases the characteristic frequencies. This result is consistent with the measurements of Springer and Thole [11], in which they observe a similar trend[3], although in general their measured frequencies are higher than those observed in our study. Fig. 12(a-b) plot the variation of wake and interior frequencies with Reynolds number for different fin thickness. Increasing thickness, decreases the wake frequency by a small amount, whereas it increases the frequency in the interior. For the 20 degree louvers there is no effect of thickness on the interior frequency. From Fig. 12(a-b) it is clear that the both the wake and interior characteristic frequencies have a very weak dependence on fin thickness, which is contrary to conventional practice for single bluff bodies. As expected, increasing the flow depth does not have a substantial effect on either the wake or the interior frequencies as seen in Fig. 12(c),

[3] Their non-dimensionalization is based on a characteristic local mean velocity at the measurement location Thus their non-dimensional frequency increases with fin pitch. Re-scaled based on our definition, the non-dimensional frequency decreases with fin pitch.

Frequency Re-Scaling

Since individual louvers are responsible for the primary instabilities that occur, it is often construed that the characteristic frequencies should scale based on some characteristic length pertaining to individual louvers, whether it be the louver length or louver thickness or some combination of the two. In previous studies, the louver thickness or more generally the fin thickness has been used as the characteristic length scale. However, the strong dependence of characteristic frequencies on fin pitch ratio in the interior clearly suggests that the fin pitch has to be taken into consideration to devise a more general non-dimensionalization for the frequency. Fin pitch potentially has one of two effects in the non-dimensionalizing of the frequency. It can be used as the characteristic length and/or its effect can be introduced in the characteristic velocity scale as in Eqn. (3). Using Eqn. (3) to reformulate the characteristic velocity and keeping the louver pitch as the characteristic length does not provide a better scaling law for the frequency. Hence, it is clear that the effect of fin pitch has to be introduced into the non-dimensionalization as a characteristic length scale. Physically, using the fin pitch as the characteristic length scale makes sense if one takes a view that the interior characteristic frequency is not a function of a single louver in isolation but rather a collection of louvers. For large fin pitches, a disturbance generated at one louver would have to travel further downstream before it interacted with another louver and hence the resulting global frequency would be lower, than if the louvers were closer as it would be for a smaller fin pitch. By re-formulating a non-dimensional frequency based on the fin pitch as the characteristic length and u_s^* as the characteristic velocity $\left(f = f^* F_p^* / u_s^*\right)$ provides a much narrower spread of interior characteristic frequencies - between 1.2 and 1.7 with a mean value at approximately 1.4. This is shown in Fig. 13(a) for all the geometries calculated. The above non-dimensionalization is also consistent with the effect of fin thickness on dimensional frequency. We note that the data of Springer and Thole [11] agrees very well with our re-scaled results, except for Re = 1000 and 1400 for F_p = 1.52, for which their re-scaled frequencies are much higher.

To develop a better scaling law for the wake frequencies we follow a slightly different tactic in defining the characteristic length. In doing so it is implicitly assumed that the exit wake instability, which occurs outside the louver bank, is fundamentally different from the interior instabilities. As illustrated earlier, the wake instability is a result of interactions between shear layers formed at the top leading edge and bottom trailing edge. Based on this observation we use the projected area of the exit louver in the flow direction as the characteristic scaling length, $L_c^* = b^* + L_p^* \sin\theta$ and characteristic velocity, u_s^*. The re-scaled wake frequencies are plotted in Fig. 13(b). The re-scaled values appear in a narrow band between 0.3 and 0.5.

Both scaling laws provided are based on observation and physical reasoning. A perfect scaling law may be very difficult if not impossible to find because of the complexity of the flow encountered and the sensitivity of the frequency to these factors. Obviously as the fin pitch increases beyond a range when two adjacent fins cease to influence each other, the interior scaling law will not be relevant. Similarly, when the exit louver departs considerably from the one used in this study, such that the formation of the wake instability changes fundamentally, the characteristic length scale may longer be valid.

NUMERICAL EXPERIMENTS

Since in all cases, the interior louver instabilities follow the exit wake instability, it would be worth investigating whether the onset of interior instabilities is influenced by the exit wake instability. If this were indeed true, then one could use the exit louver to control the onset of instabilities in the interior of the array. Equally important is the knowledge of what effect, if any, does the exit louver have on the interior propagation of instabilities and on the characteristic frequencies. Conversely, albeit secondary in nature, is the effect of the interior louver geometry on the exit wake instability. We answer these questions by doing a series of numerical experiments at selected Reynolds numbers, which are outlined in Table 2. In the first set we vary the angle of the exit louver – from 30 to 15 degrees for case 5 in Table 1 and from 20 degrees to 30 degrees for case 7. In the second set of experiments, we completely eliminate the exit louver in case 1 and 5 from Table 1.

Effect of Exit Wake Instability on Internal Array Instability

This is best answered by considering the two cases in which the exit louver is removed from the calculation. In the base calculations with exit louver included, exit wake instabilities appeared at Re_{in} = 400 and interior instabilities began to appear at Re_{in} = 700. However, in the numerical experiments without the exit louver, no instabilities developed at Re_{in} = 400 in the wake of the fin and the flow remained stable for both cases. In spite of this, interior instabilities were found to develop at the same Reynolds number of Re_{in} = 700 for both cases. In addition, the characteristic frequencies and the propagation of instabilities into the interior were identical to the base cases. These results establish without any doubt that the internal array instabilities are completely independent of the exit wake instability.

Effect of Interior Louver Geometry on Exit Wake Instability

For case 7 (F_p = 1.5, θ=20 degrees), the exit wake instability appears at Re_{in} = 800 followed by the interior instability at Re_{in} = 1000. If the exit wake instability were only dependent on the exit louver geometry, then changing the exit louver angle from 20 to 30 degrees would initiate the wake instability at Re_{in} = 400. However, we observe that the wake instability develops at Re_{in} = 500, which, in fact shows a strong dependence on the exit louver geometry. Conversely, in case 5 (F_p = 1.5 , θ= 30 degrees), the exit wake instability appears at Re_{in} = 400 with the interior instability following at Re_{in} = 700. For 15 degree louvers (case 8, F_p = 1.5), the corresponding wake instability appears as late as Re_{in} = 1200. By changing the exit louver angle to 15 degrees, the wake instability is only delayed to Re_{in} = 600, which shows a strong preference for the internal louver geometry. Hence, in this case the effect of louver geometry upstream of the exit louver has a much more dominant effect on the initial appearance of the wake instability. In spite of the wake instability appearing later at Re_{in} = 600, the interior instability appears at 700 as in the base case, which confirms our earlier observation that the exit wake instability has no effect on the interior instability.

SUMMARY AND CONCLUSIONS

The paper describes the transition mechanism in multilouvered fin geometries by studying the effect of fin pitch ratio, louver angle, fin thickness ratio, and flow depth on the onset, propagation and characteristic frequencies. Instabilities are always found to develop first in the wake of the exit louver, which then spread upstream into the louver bank. In spite of this, it is shown through numerical experiments that the interior louver bank instabilities (initiation, propagation and frequencies) are completely independent of the exit wake instability. Conversely, the exit wake instability is not only dependent on the exit louver geometry, but also on the upstream geometry of the louver bank.

Based on these observations, we provide a simplified technique for estimating the onset of internal array instabilities. It is assumed that the flow through the louvers is similar to a duct flow with louvers acting as roughness elements, which perturb the flow till it becomes unstable. This is quantified by defining a critical Reynolds number based on the flow distance traversed.

Louver angle and louver thickness have the largest effect on the onset of the exit wake and internal louver bank instabilities - large angles and thicker fins exhibit an earlier onset of instabilities. The effect of fin pitch on the onset is weak. However, the rate of propagation of instabilities into the louver bank is much higher for large fin pitches and large louver angles. Increasing the louver thickness ratio also enhances the propagation of instabilities.

We show that the characteristic frequencies in the exit wake and internal to the louver bank scale on different length scales. The frequencies in the exit wake scale on a characteristic length scale pertaining to the projected length of the exit louver in the flow direction, whereas the internal array frequencies scale better with fin pitch rather than characteristic length scales pertaining to individual louvers.

ACKNOWLEDGEMENTS

During this study, Dr. X. Zhang supported by the Air Conditioning and Refrigeration Center, Department of Mechanical and Industrial Engineering, University of Illinois, Urbana Champaign and by a NSF fellowship under grant ASC 94-04934. Supercomputing time was granted by the NSF PACI program through the National Resource Allocation Committee (NRAC).

REFERENCES

1. C. J. Davenport, Heat Transfer and Flow Friction Characteristics of Louvered Heat Exchanger surfaces, *Heat Exchangers: Theory and Practice*, Taborek, J., Hewitt, G. F. and Afgan, N. (eds.), pp. 397-412, Hemisphere, Washington, D. C., 1983.

2. R. L. Webb, and P. Trauger, Flow Structure in the Louvered Fin Heat Exchanger Geometry, *Experimental Thermal and Fluid Science*, Vol. 4, pp. 205-217, 1991.

3. K. Suga, and H. Aoki, Numerical Study on Heat Transfer and Pressure Drop in Multilouvered Fins, *ASME/JSME Thermal Engineering Proceedings*, Vol. 4, pp. 361-368, 1991.

4. X. Zhang and D. K. Tafti, Classification and effects of thermal wakes on heat transfer in multilouvered fins, submitted *Int. J. Heat Mass Transfer*, April 2000.

5. L. W. Zhang, D. K. Tafti, F. M. Najjar, and S. Balachandar, Computations of Flow and Heat Transfer in Parallel-Plate Fin Heat Exchangers on the CM-5: Effects of Flow Unsteadiness and Three-Dimensionality, *Int. J. Heat Mass Transfer*, Vol. 40, pp. 1325-1341, 1997.

6. L. W. Zhang, S. Balachandar, D. K. Tafti, and F. M. Najjar, Heat Transfer Enhancement Mechanisms in Inline and Staggered Parallel-Plate Fin Heat Exchangers, *Int. J. Heat Mass Transfer*, Vol. 40, No. 10, pp. 2307-2325, 1997.

7. S. Mochizuki and Y. Yagi, Characteristics of Vortex Shedding in Plate Arrays, in Flow Visualization II, ed. W. Merzkirch. Washington, DC, hemisphere, pp. 99-103.

8. N. C. Dejong and A. M. Jacobi, An experimental study of flow and heat transfer in parallel-plate arrays: local, row-by-row and surface average behavior, *Int. J. Heat Mass Transfer*, Vol. 40, No. 6, pp. 1365-1378, 1997.

9. N. C. Dejong and A. M. Jacobi, Flow, Heat Transfer, and Pressure Drop Interactions in Louvered-Fin Arrays, ACRC TR-146, University of Illinois, Mechanical and Industrial Engineering Dept., Jan. 1999.

10. M. E. Springer and K. A. Thole, Experimental design for flowfield studies of louvered fins, *Experimental Thermal and Fluid Science* 18, pp. 258-269, 1998.

11. M. E. Springer and K. A. Thole, Entry region of louvered fin heat exchangers, *Experimental Thermal and Fluid Science* 19, pp. 223-232, 1999.

12. D. K. Tafti, G. Wang and W. Lin, Flow transition in a multilouvered fin array, *Int. J. Heat Mass Transfer,* 43, pp. 901-919, 2000.

13. D. K. Tafti, L. W. Zhang and G. Wang, Time-Dependent Calculation Procedure for Fully Developed and Developing Flow and Heat Transfer in Louvered Fin Geometries, *Num. Heat Transfer, Part A*, 35:225-249, 1999.

14. D. K. Tafti, X. Zhang, W. Huang, G. Wang, Large-Eddy Simulations of Flow and Heat Transfer in Complex Three-Dimensional Multilouvered Fins, Invited paper, paper No. FEDSM2000-11325, CFD Applications in Automotive Flows, 2000 ASME Fluids Engineering Division Summer Meeting, June 11-15, Boston, Massachusetts, 2000.

Table 1: Summary of non-dimensional geometrical parameters for the cases investigated.

Case	F_p	θ	b	F_d
1-a	1.0	30	0.05	19
1			0.1	
1-b			0.15	
2	1.0	25	0.1	19
3-a	1.0	20	0.05	19
3			0.1	
3-b			0.15	
4	1.0	15	0.1	19
5	1.5	30	0.1	19
5-a				23
6	1.5	25	0.1	19
7	1.5	20	0.1	19
8	1.5	15	0.1	19

Table 2: geometrical parameters for instability experimental calculations,

Set	F_P	θ	θ_{exit}	Re_{in}
1	1.0	30	No exit	400, 700, 800, 900, 1000, 1300
	1.5		louver	400, 700, 800, 1000, 1300
2	1.5	30	15	600, 700, 800, 1000
		20	30	400, 500, 800, 1200

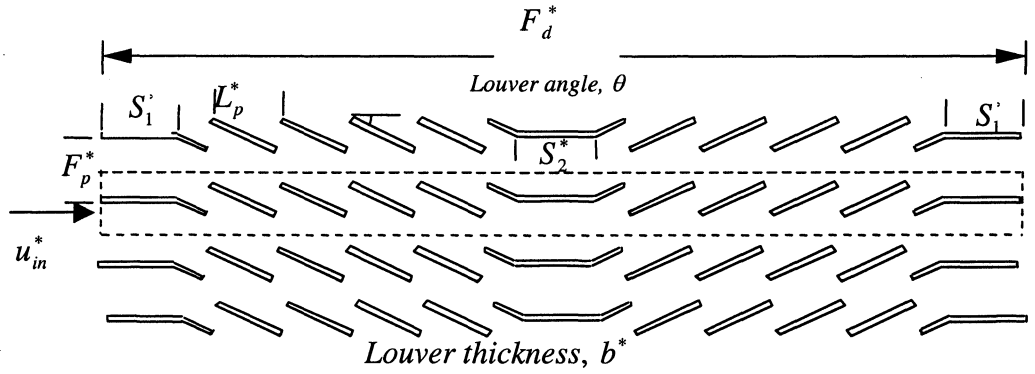

(a)

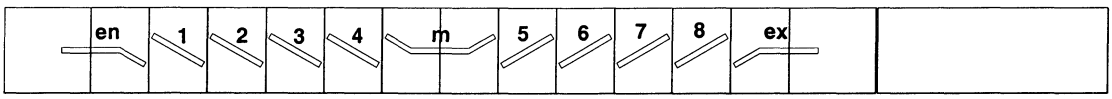

(b)

Figure 1: (a) Geometry of multilouvered fins; (b) Typical calculation domain resolved with multiple computational blocks. Each block is resolved by 96x96 computational cells.

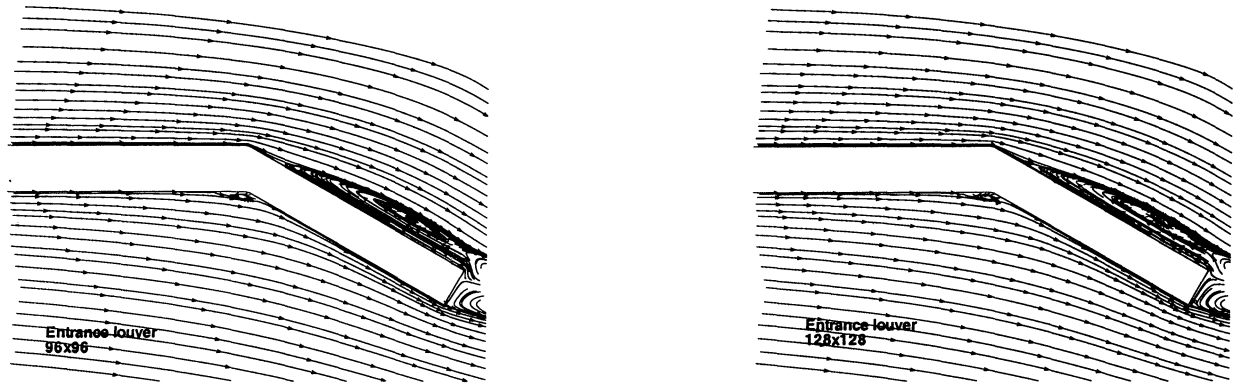

(a)

(b)

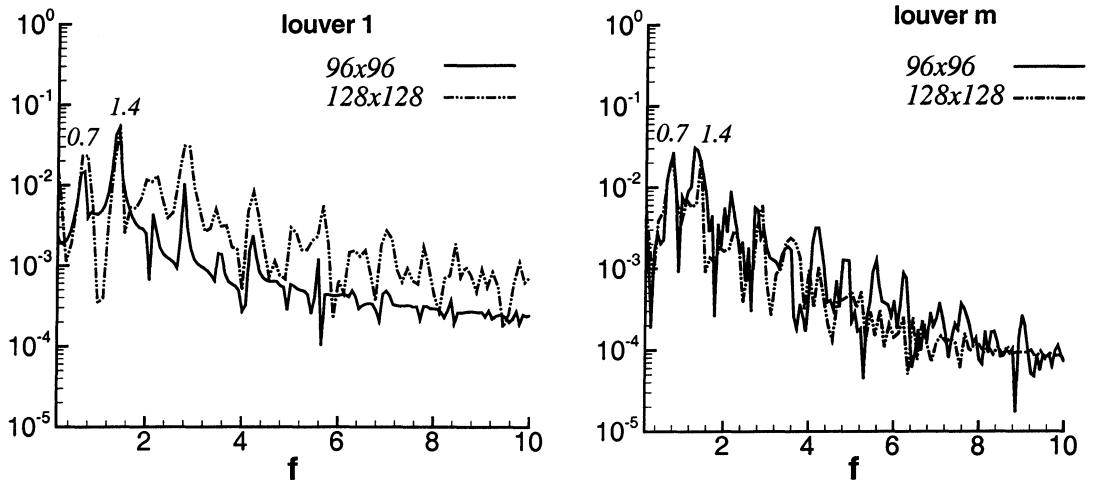

(c) (d)

Figure 2: Grid Independency: (a) Comparison of mean streamlines on the entrance louver and louver 5 behind the re-direction louver; (b) Comparison of frequency spectra and characteristic frequencies.

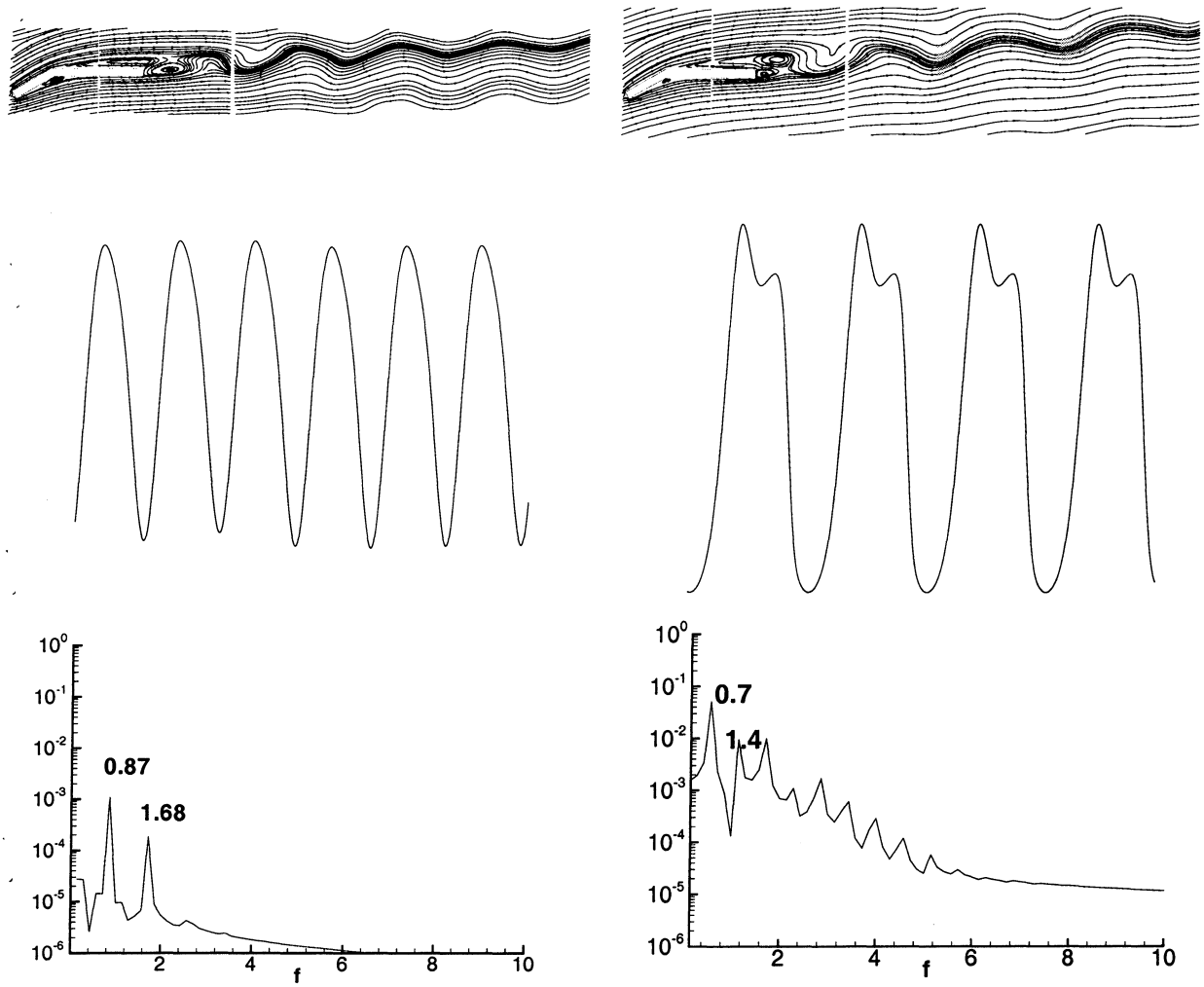

Figure 3: Formation of the exit instability, time signal of temperature and frequency spectra for two louver geometries: (a) F_p = 1.0, θ = 30 degrees, b = 0.1; (b) F_p = 1.5, θ = 30 degrees, b = 0.1.

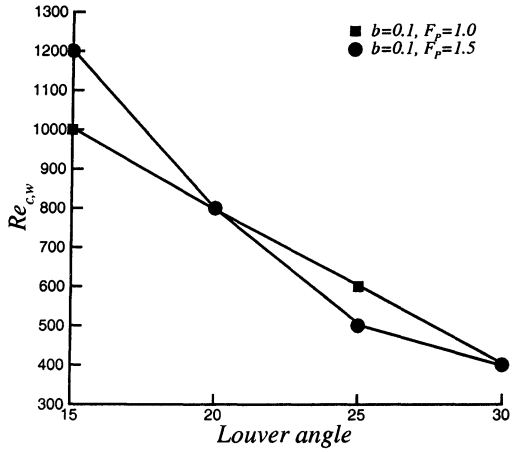

(a)

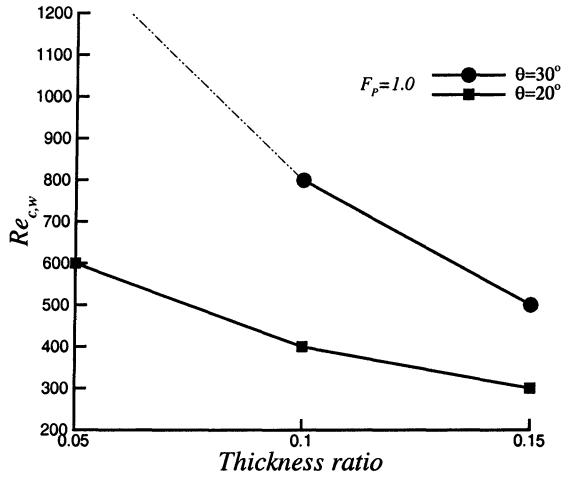

(b)

Figure 4: Exit wake critical Reynolds number: (a) Effect of fin pitch and louver angle; (b) effect of louver thickness.

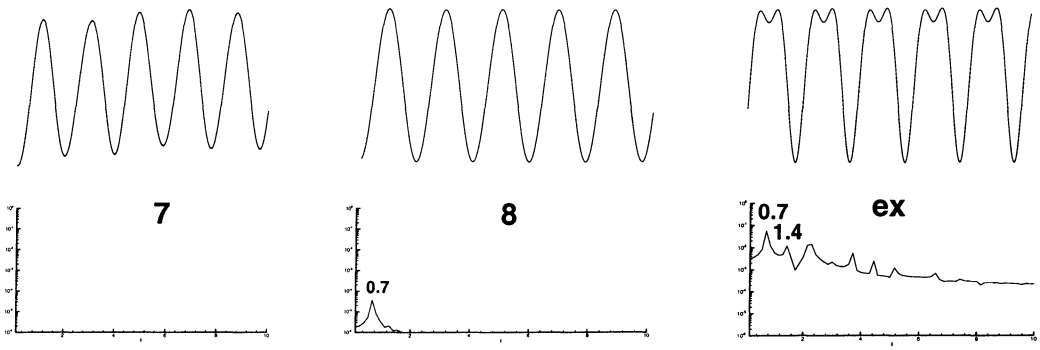

(a)

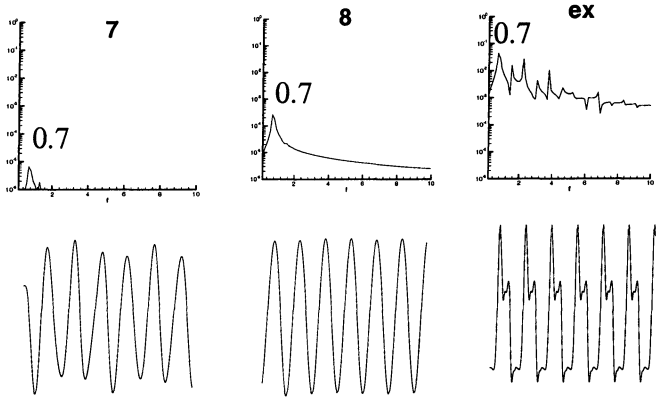

(b)

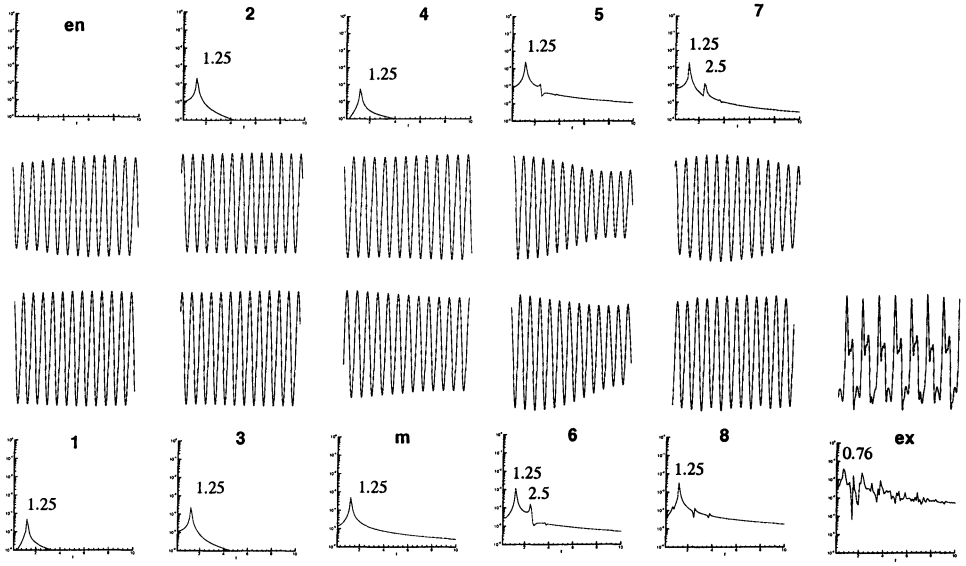

(c)

Figure 5: Penetration of exit wake characteristic frequency into interior of louver bank for F_p = 1.5, θ = 30 degrees, b = 0.1: (a) Re_{in} = 500; (b) Re_{in} = 600; (c) Onset of interior instability, Re_{in} = 700.

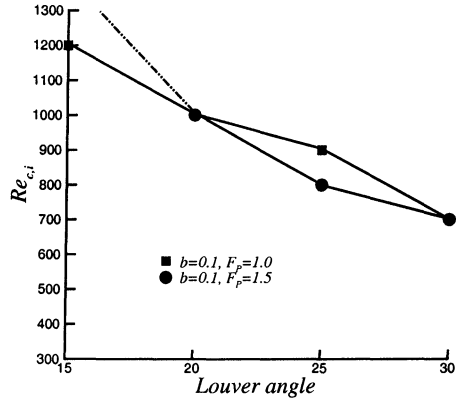

(a)

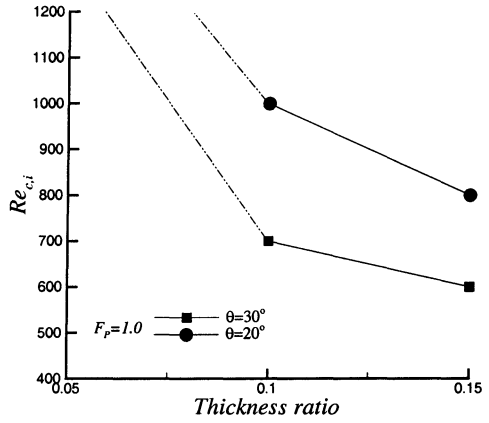

(b)

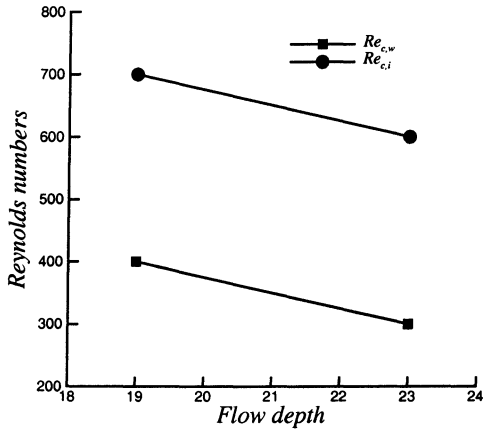

(c)

Figure 6: Interior critical Reynolds number : (a) Effect of fin pitch and louver angle; (b) effect of louver thickness; (c) effect of flow depth on exit wake and interior onset of instabilities.

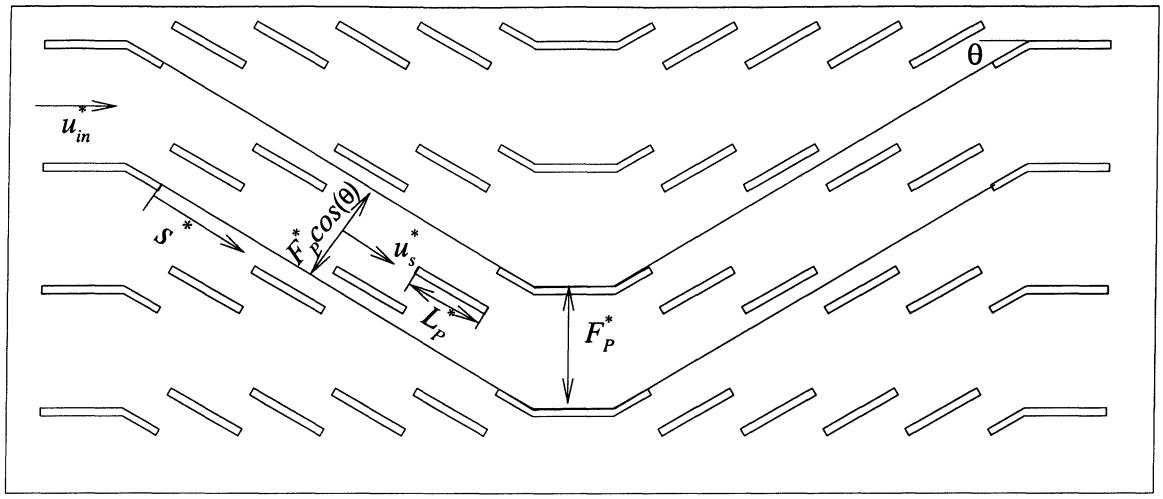

(a)

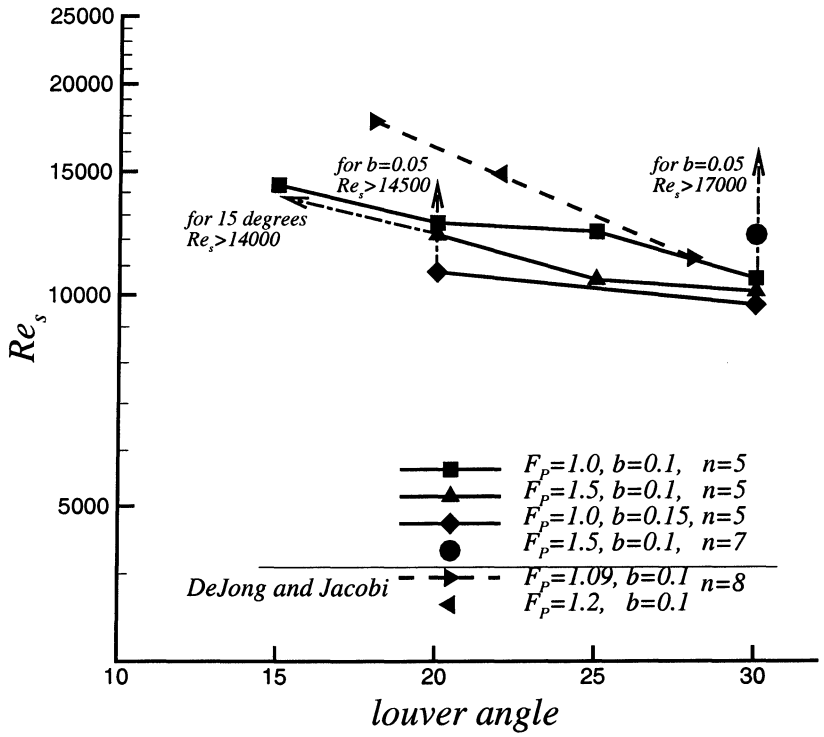

(b)

Figure 7: (a)Schematic of flow path traversed by fluid element used in the definition of Re_s; (b)Critical Reynolds based on Re_s for all computations and flow visualization studies of Dejong and Jacobi [9].

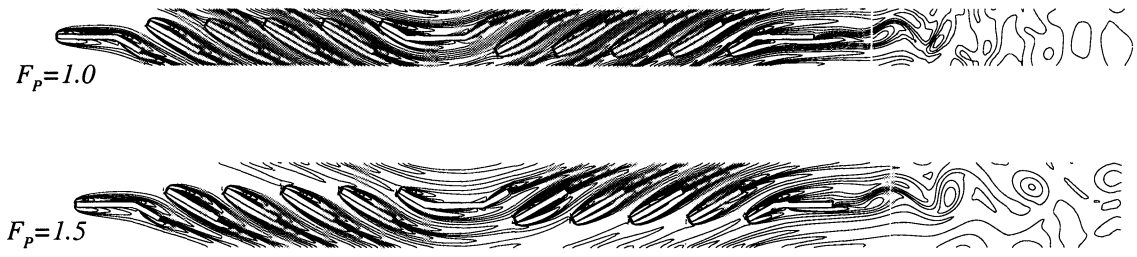

(a)

(b)

Figure 8: Instantaneous vorticity contours illustrating rate of propagation of instabilities into interior of louver bank for θ = 30 degrees, b = 0.1, and F_p = 1.0 and 1.5.

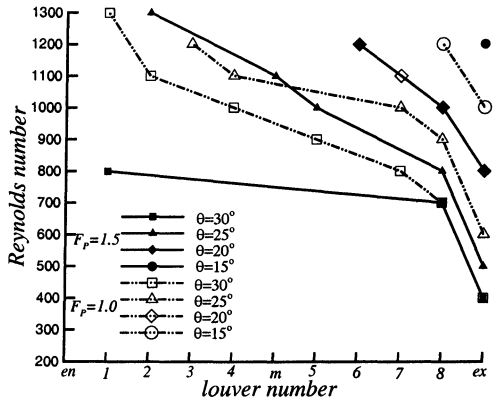

(a)

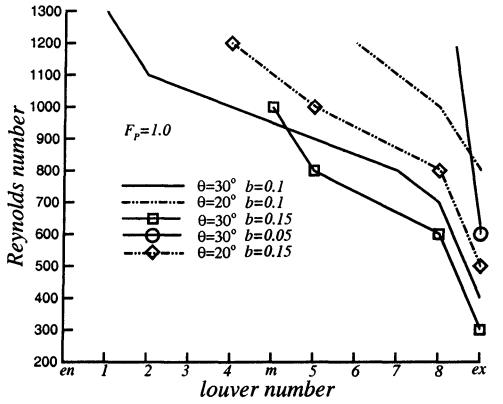

(b)

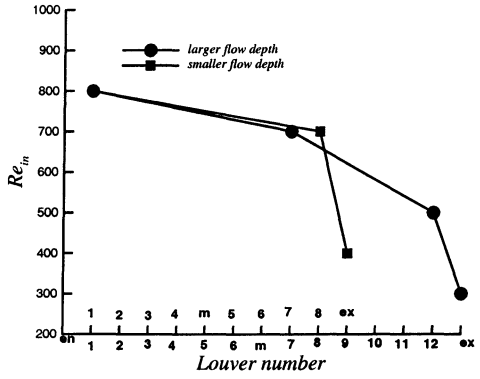

(c)

Figure 9: Summary of rate of propagation of instabilities into louver bank: (a) effect of fin pitch and louver angle; (b) effect of louver thickness; (c) effect of flow depth.

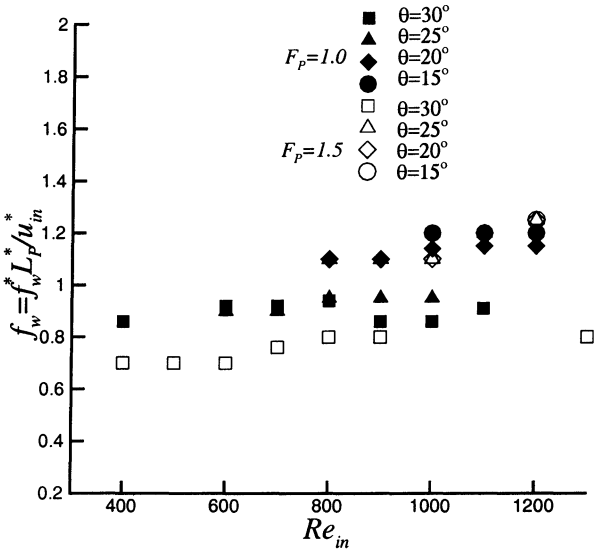

(a)

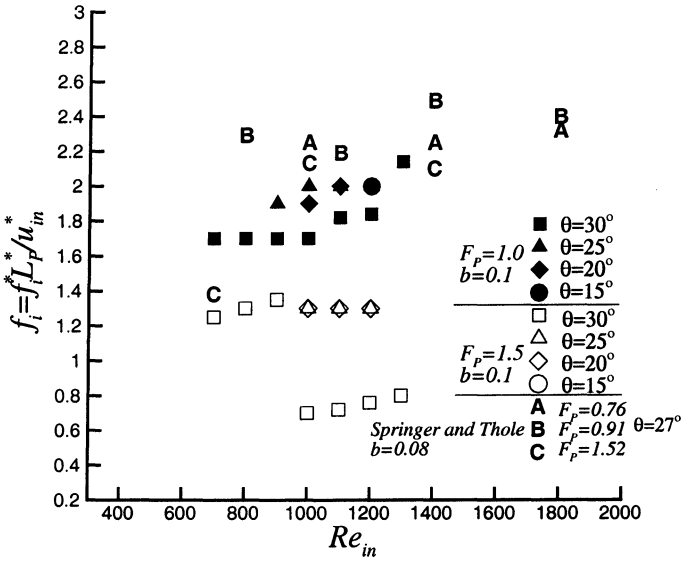

(b)

Figure 10: Characteristic non-dimensional frequencies from computations and experiments of Springer and Thole [11]. Effect of fin pitch and louver angle: (a) exit wake; (b) interior of louver bank.

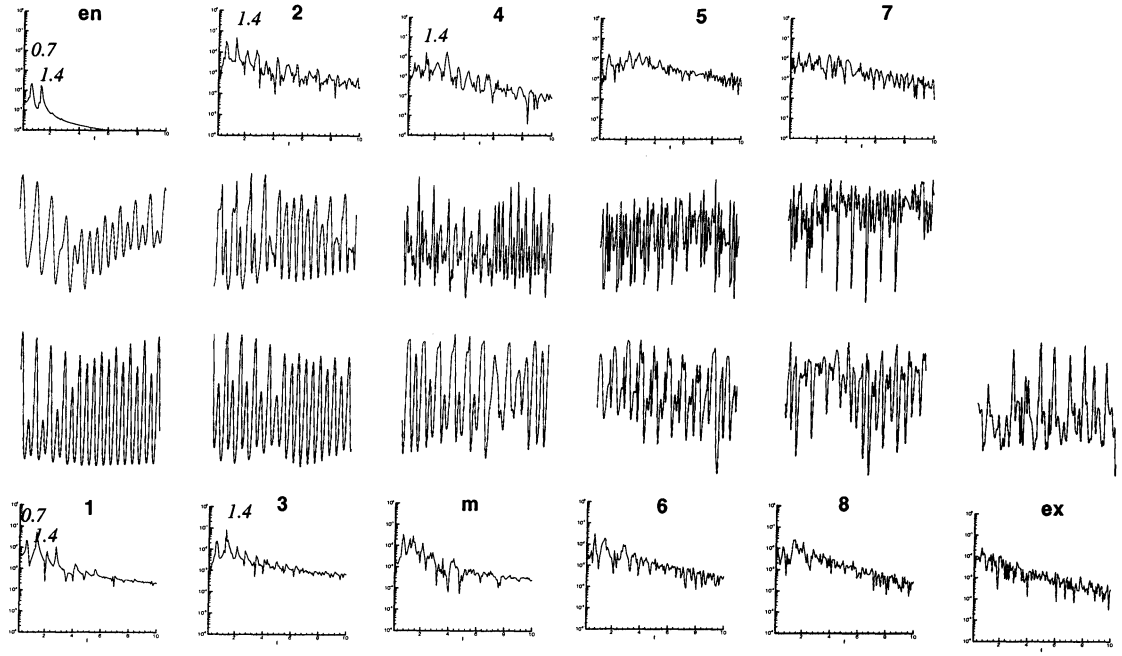

(a)

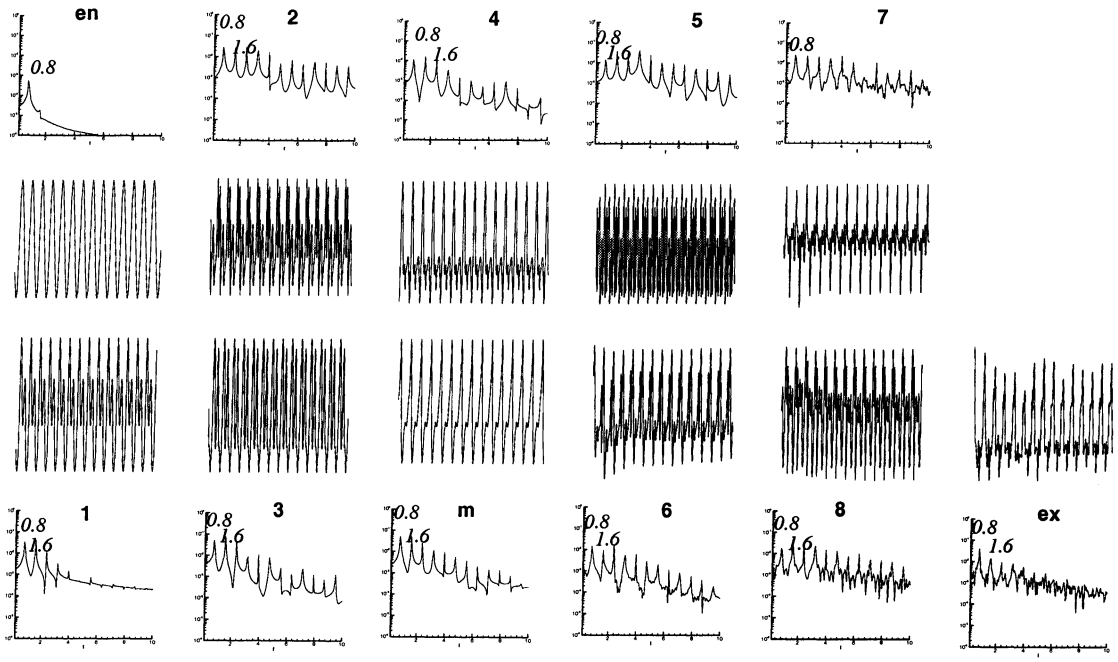

(b)

Figure 11: Characteristic frequencies and period doubling observed between (a) Re_{in} = 1000 and (b) Re_{in} = 1300 for F_p = 1.5, θ = 30 degrees and b = 0.1.

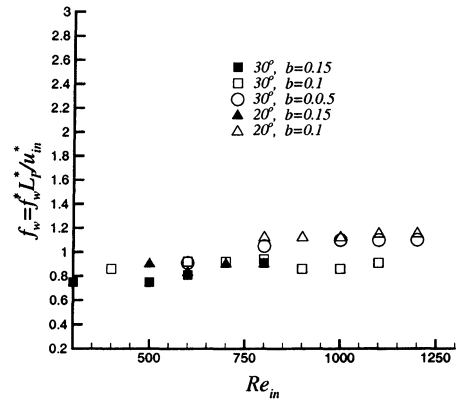

(a)

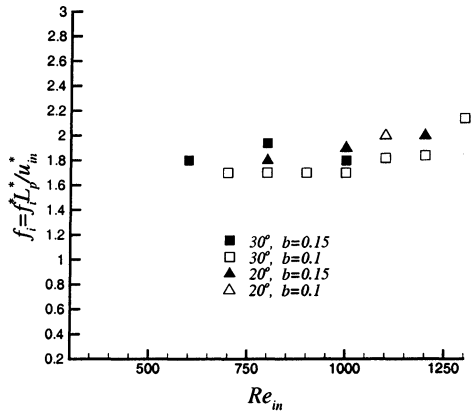

(b)

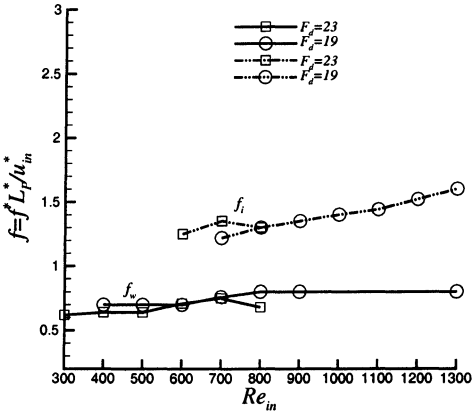

(c)

Figure 12: Characteristic non-dimensional frequencies. Effect of louver thickness: (a) Exit wake; (b) interior of louver bank; (c) effect of flow depth on exit wake and interior frequencies.

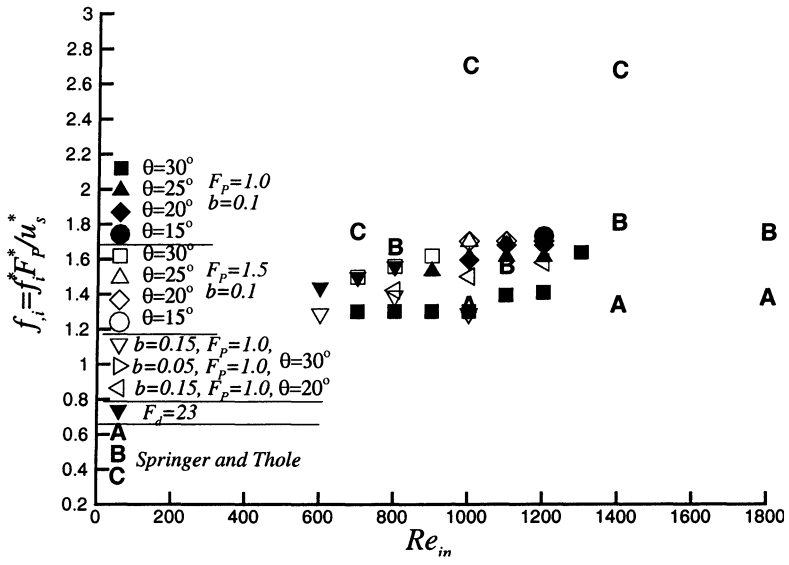

(a)

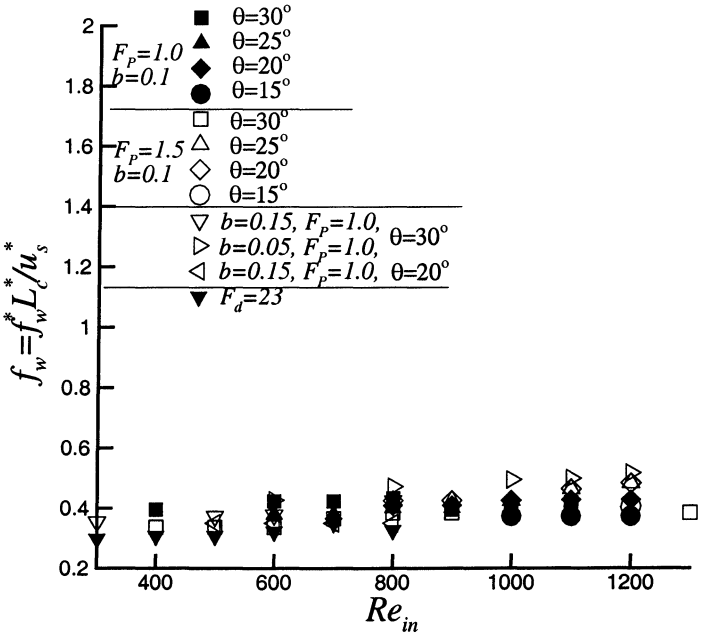

(b)

Figure 13: Re-scaled characteristic frequencies: (a) interior of louver bank; (b) exit wake.